ISIJ International, Vol. 57 (2017), No. 9, pp. 1586–1594

Roughing of Thick, Coarse-grained High-temperature-processing Steels Processed via Compact Strip Production

Kevin Mark BANKS,* Alison Susan TULING and Dannis Rorisang Nkarapa MAUBANE

University of Pretoria, Private Bag X20, Hatfield, 0028 South Africa.

(*Received on March 3, 2017; accepted on May 25, 2017*)

The roughing conditions required to avoid local heterogeneous regions in the final microstructure of high temperature processing (HTP) Nb linepipe steels have been investigated for quasi-compact strip production (CSP) conditions. The influence of strain sequence, rolling temperatures and Mn content on recrystallisation and carbonitride precipitation before and after roughing were studied using laboratory simulation, mathematical modelling and transmission electron microscopy. The roughing conditions necessary to avoid the formation of local heterogeneous regions have been established for HTP steels with an initial grain size of 850 μm. Low Mn Nb–Ti steels experience more sluggish recrystallisation kinetics and are more vulnerable to forming local heterogeneous regions during roughing. To prevent local heterogeneous regions if finishing commences at 900°C, sufficient effective strain is necessary to produce a bulk softened fraction of at least 0.55 in each of the first two roughing passes. If finishing commences at 1 000°C, slow air cooling from roughing provides additional time for recrystallisation to go to completion and so prevent the occurrence of local heterogeneous regions. Maintaining the strand temperature as high as possible prior to the commencement of roughing encourages recrystallisation. A roughing start temperature of 1 100°C, as opposed to 1 075°C, significantly reduces the risk of forming local heterogeneous regions. For the conditions tested, no correlation between softening fraction and carbonitride precipitate characteristics was found. Thus, the influence of Nb on austenite recrystallisation is expected to be due to either solute drag or solute clustering.

KEY WORDS: CSP; roughing; niobium; manganese; recrystallisation; precipitation; local heterogeneous regions.

1. Introduction

Local heterogeneous regions are hard, elongated regions in the final ferrite-pearlite microstructure of microalloyed steels which form during cooling from coarse, unrecrystallised austenite. They are a result of steel composition (mainly Nb and C) and inadequate thermomechanical processing during high temperature processing, *i.e.*, small strains, too low roughing temperatures and short inter-pass times.[1–5] If present in sufficient quantities, local heterogeneous regions can impair toughness.[4] Nb microalloyed steels are most sensitive to this behaviour because of strong solute drag and Nb(C,N) precipitation effects capable of retarding static recrystallisation during initial rolling.[4] Thus, in CSP, two distinct objectives must be met when defining rolling schedules: i) elimination of the coarse initial grains and local heterogeneous regions during and immediately after roughing through recrystallisation and ii) once achieved, obtain a pancaked austenite microstructure during finishing which is saturated with dislocations prior to transformation. These aims are more challenging in the production of thick skelp since the total applied reduction is limited.

The concept of low Mn additions to high Nb–Ti sour service HTP linepipe steels has recently been introduced to improve centreline segregation and inclusion shape control.[6] For a given base chemistry and at sufficiently low temperatures, high Nb contents provide a large supersaturation and chemical driving force for fine precipitation to effectively retard the austenite recrystallisation kinetics via grain boundary pinning.[4] In addition, Akben *et al.*[7] reported that for a given Nb content, low Mn (also Mo, V) contents retard recrystallisation. At finishing temperatures, low Mn contents accelerate strain-induced precipitation of Nb and restrict grain boundary movement,[8] thereby increasing the so-called no-recrystallisation temperature, T_{NR}, and promotes austenite grain pancaking. Although Nb(C,N) precipitation may occur at higher, roughing temperatures in these steels, the particles may be too coarse for effective grain boundary pinning and reduce the solute content which accelerate recrystallisation. However, the influence of Mn content and Nb carbonitride precipitation on recrystallisation kinetics in the high temperature austenite region of these steels under CSP (coarse-grained) conditions have not been quantified. This work aims to i) determine the effect of precipitation on recrystallisation in the roughing stage of CSP and ii) quantify, through the use of physical simulation and mathematical models, the required roughing conditions

* Corresponding author: E-mail: kevin.banks@up.ac.za
DOI: http://dx.doi.org/10.2355/isijinternational.ISIJINT-2017-105

to produce a microstructure free of local heterogeneous regions in both high and low Mn HTP steels.

2. Experimental and Modelling

2.1. Physical Simulation

Table 1 shows the chemistry of two HTP steels investigated: a conventional high Mn, - high Nb grade, *HMn*, and a low Mn - high Nb steel *LMn*, with the as received microstructures in **Fig. 1**. **Figure 2** details rolling schedules A-C that were performed in a Bahr 805D deformation dilatometer under quasi-CSP conditions through soaking at 1 400°C to produce an average initial grain size, d_0, of 850 μm.[1–3] The soaking temperature was decreased in schedule A1 to establish the influence of initial condition on local heterogeneous regions, *i.e.*, cold-charge rolling (CCR) at 1 290°C to produce a d_0 of 125 μm.[1–3] In schedule C, the roughing start temperature was varied between 1 075°C (C1) and 1 100°C (C2). All tests included an initial cool into the lower austenite region (T_{min}), except in schedule C3, where cooling was applied directly to the equalising furnace temperature (1 100°C). Intermediate accelerated cooling was applied at 14°Cs^{-1} when the finishing entry temperature, F1, was 900°C, whilst an air cooling rate (0.5°Cs^{-1}) was applied when F1 was 1 000°C. After deformation, specimens were accelerated cooled to 600°C and held for 5 min. to finally examine the "as-coiled" microstructure using a 2% nital solution. The measured softened (*i.e.*, recovery and recrystallisation) fraction, X_M, between passes was determined from the resulting flow curves using the 0.2% offset method.

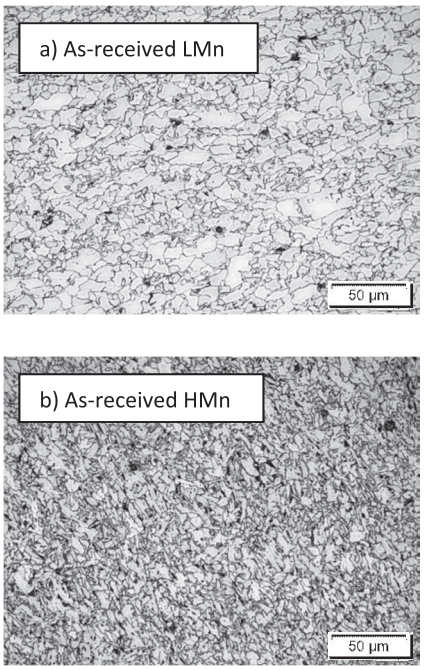

Fig. 1. As-received microstructures of a) LMn and b) HMn steels produced via CCR.

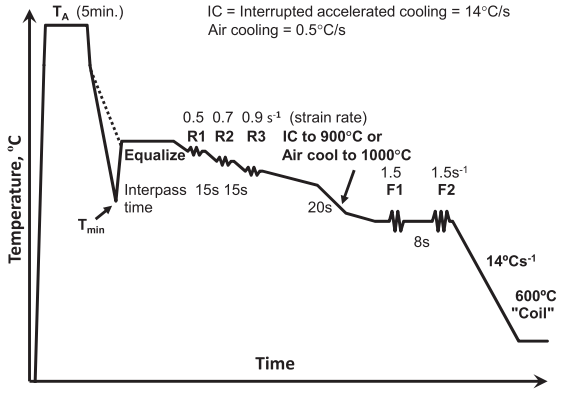

Sch.	T_A	T_{min}	Equal.	Applied strains R1	R2	R3	Rolling Temperatures,°C F1	R1	R2	R3	F1
A1:	1290	950	1100	0.24	0.17	0.17	0.29	1075	1050	1025	900
A2:	1400	950	1100	0.24	0.17	0.17	0.29	1075	1050	1025	900
B:	1400	950	1100	0.12	0.51	-	0.29	1075	1050	1025	900
C1:	1400	950	1100	0.40	0.22	0.11	0.29	1075	1050	1025	900/1000
C2:	1400	950	1125	0.40	0.22	0.11	0.29	1100	1075	1050	900
C3:	1400	-	1100	0.40	0.22	0.11	0.29	1075	1050	1025	900

Fig. 2. Schematic of CSP simulations.

To follow the precipitation evolution in the early stages of processing, additional specimens were quenched directly after i) T_{min}, ii) equalizing at 1 100°C, iii) pass R1 and iv) R3, from which carbon extraction replicas were prepared for analytical TEM. The diameters, d_p, of more than 140 particles were measured in each population, while the particle density was estimated from the nearest neighbour distance, L. Plate-like eutectic precipitation of Nb, which had a limited presence, was ignored for L and d_p measurements.

2.2. Recrystallisation Model

Table 2 is a collection of isothermal equations that describe the evolution of coarse-grained austenite in Nb–Ti steels which were employed here: d_0, ε_{eff}, $\dot{\varepsilon}$, t and T are the initial austenite grain size, effective von Mises strain that includes any accumulation from previous passes, average strain rate, inter-pass time and pass temperature respectively. For simplicity, where non-isothermal conditions prevailed, *i.e.*, between passes, the average temperature was used. If ε_{eff} exceeded the critical strain for dynamic recrystallisation, ε_c, then the metadynamic recrystallisation, MDRX, equations were applied. Static recrystallization (SRX) however, was the dominant softening mechanism. The constant C in Eq. (2) is quoted as 9.92×10^{-11} s but was later modified based on the results found here. The model includes the effect of solute Nb and Ti on recrystallization kinetics but not Mn, Si, V and Mo which are known to affect the rate of softening processes.[7] The equilibrium solute contents in multi-component austenite at the equalising temperature was calculated using Thermocalc® and, considering that cooling retards precipitation, were assumed constant during roughing.

Table 1. Composition of steels studied - mass% (V < 0.001%, Mo < 0.01%).

Steel	C	Mn	Si	Nb	Ti	Cr	Ni	Cu	P	Al	N	S
HMn	0.050	1.59	0.16	0.099	0.010	0.24	0.11	0.22	0.019	0.039	0.0039	0.0080
LMn	0.054	0.25	0.16	0.088	0.010	0.48	0.16	0.29	0.016	0.033	0.0032	0.0001

Table 2. Equations describing austenite evolution in Nb–Ti steels.

Variable, pass i	Ref	Equation	Eq.
Critical strain for DRX	10	$\varepsilon_c = 0.0016\left(1+20[\mathrm{Nb}]+0.02[\mathrm{Ti}]\right)d_0^{0.147}Z^{0.155}, \quad Z=\dot{\varepsilon}\exp\left(\frac{325\,000}{RT}\right)$	1
Time for 50% SRX	9	$t_{0.5SRX} = Cd_0\varepsilon_{eff}^{-5.6d_0^{-0.15}}\ \dot{\varepsilon}^{-0.53}\exp\left(\frac{180\,000}{RT}\right)\exp\left(\left(\frac{275\,000}{T}-185\right)\left([\mathrm{Nb}]+0.374[\mathrm{Ti}]\right)\right)$	2
Time for 50% MDRX	10	$t_{0.5MDRX} = 1.77\times10^{-6}\dot{\varepsilon}^{-0.62}\exp\left(\frac{153\,000}{RT}\right)$	3
SRX grain size	11	$d_{SRX} = 1.4d_0^{0.56}\varepsilon_{eff}^{-1}$	4
MDRX grain size	12	$d_{MDRX} = 1\,370\left(\dot{\varepsilon}\exp\left(\frac{375\,000}{RT}\right)\right)^{-0.13}$	5
Mean d_{rex}	13	$d_{rex,i} = d_{r,SRX}.X_{SRX} + d_{r,MDRX}.X_{MDRX}$ with $d_{r,SRX,MDRX} = d_{SRX,MDRX}.X_{SRX,MDRX}^{1/3}$	6
Mean incoming grain size	14	$d_{0,i} = d_{rex,i}X_i^{4/3} + d_{0,i-1}\left(1-X_i\right)^2$	7
Fraction recrystallised	10	$X = X_{SRX} + X_{MDRX}, \quad X_{SRX,MDRX} = f_{MDRX,SRX}\left\{1-\exp\left[-0.693\left(\frac{t}{t_{0.5SRX,MDRX}}\right)\right]\right\}$	8
Contributed fraction	10	$f_{MDRX} = \frac{\varepsilon_{eff}-\varepsilon_c}{1.2}, \quad f_{SRX} = 1-f_{MDRX}$	9
Effective strain	14	$\varepsilon_{eff,i} = \varepsilon_i + (1-X_{i-1})\,\varepsilon_{i-1}$	10

3. Results

3.1. Bahr Deformation Dilatometer CSP Simulations

The flow curves and X_M values after each pass are plotted in **Fig. 3** for all schedules that included an F1 temperature of 900°C. Figure 3(a) are results from CCR simulations and Figs. 3(b)–3(f) are for CSP tests. The predicted softened fraction, X_C, and average incoming grain size, $d_{0,i}$, after pass i are also shown and discussed in section 4.3. The corresponding "as-coiled" microstructures resulting from the simulations in Fig. 3 are shown in **Fig. 4**, where the *HMn* steel generally displayed a finer microstructure due to its lower transformation temperature.[2] Regions considered to be "local heterogeneous regions" are elongated regions which differ considerably in aspect ratio from the matrix. A SEM micrograph of a typical local heterogeneous region in *LMn* steel is shown in **Fig. 5**. Two types of local heterogeneous region morphology were identified: fine ferritic and bainitic. **Figures 6** and **7** show the thermomechanical behaviour and resulting microstructure for an F1 of 1 000°C in schedule C1. The general observations in Figs. 3–7 are:

- The *LMn* steel matrix consisted of mixed, coarse polygonal ferrite with little or no pearlite. Local heterogeneous regions in the *LMn* grade were either very fine, elongated ferrite or low carbon bainite. The *HMn* matrix was fine ferrite with 5% pearlite and, where present, the local heterogeneous regions contained relatively coarse, acicular ferrite-pearlite.
- No local heterogeneous regions were observed in the microstructure when X_M exceeded 0.55 in the first (R1) roughing pass and at least one subsequent pass. The calculated grain size entering pass R2, $d_{0,2}$ was always below about 200–220 μm in local heterogeneous region-free specimens.
- X_M was mostly lower in the *LMn* steel for a given rolling schedule suggesting more sluggish recrystallisation compared to *HMn*.
- The local heterogeneous regions were similar to the matrix morphology in the HMn steel. The morphology of local heterogeneous regions in the *LMn* steel was distinctly different to its matrix and very elongated.

In CCR schedule A1, X_M values above 0.55 were obtained after passes R1 and R2 with no evidence of local heterogeneous regions, Fig. 4(a). The $d_{0,2}$ was 45 μm. In CSP schedule A2, the small applied strains in R1 and R2 resulted in X_M below 0.55 in all passes except R2 and large local heterogeneous regions were observed in both steels, Fig. 4(b). In schedule B, a small reduction in R1, followed by a large strain in R2 (applied strain of 0.51 and accumulated strain from R1) was sufficient to initiate MDRX (confirmed by the presence of a peak stress), but was unsuccessful in avoiding local heterogeneous regions, Fig. 4(c). The $d_{0,2}$ in these two schedules was very coarse - 500 to 800 μm. The roughing strain sequence in schedule C1 commencing at 1 075°C resulted in an X_M just below 0.55 and a $d_{0,2}$ of 223 μm. Local heterogeneous regions were more prominent in *LMn* grade than in *HMn*, Fig. 4(d). Local heterogeneous regions were eliminated in both steels i) when roughing temperatures were increased by 25°C in schedule C2, Fig. 4(e) and ii) when cooling was applied directly to the equalising temperature in schedule C3 as opposed to initially cooling to T_{min} (Fig. 2), despite deformation commencing at 1 075°C, Fig. 4(f). The $d_{0,2}$ was 129 and 146 μm in schedules C2 and C3 respectively.

Raising the F1 temperature to 1 000°C following a slow air cool from the end of roughing had a positive effect in eliminating local heterogeneous regions in both grades, Figs. 6–7, indicating that high X_M values in subsequent passes, even as late as F1, assist in the elimination of local heterogeneous regions. The *LMn* steel matrix was similar

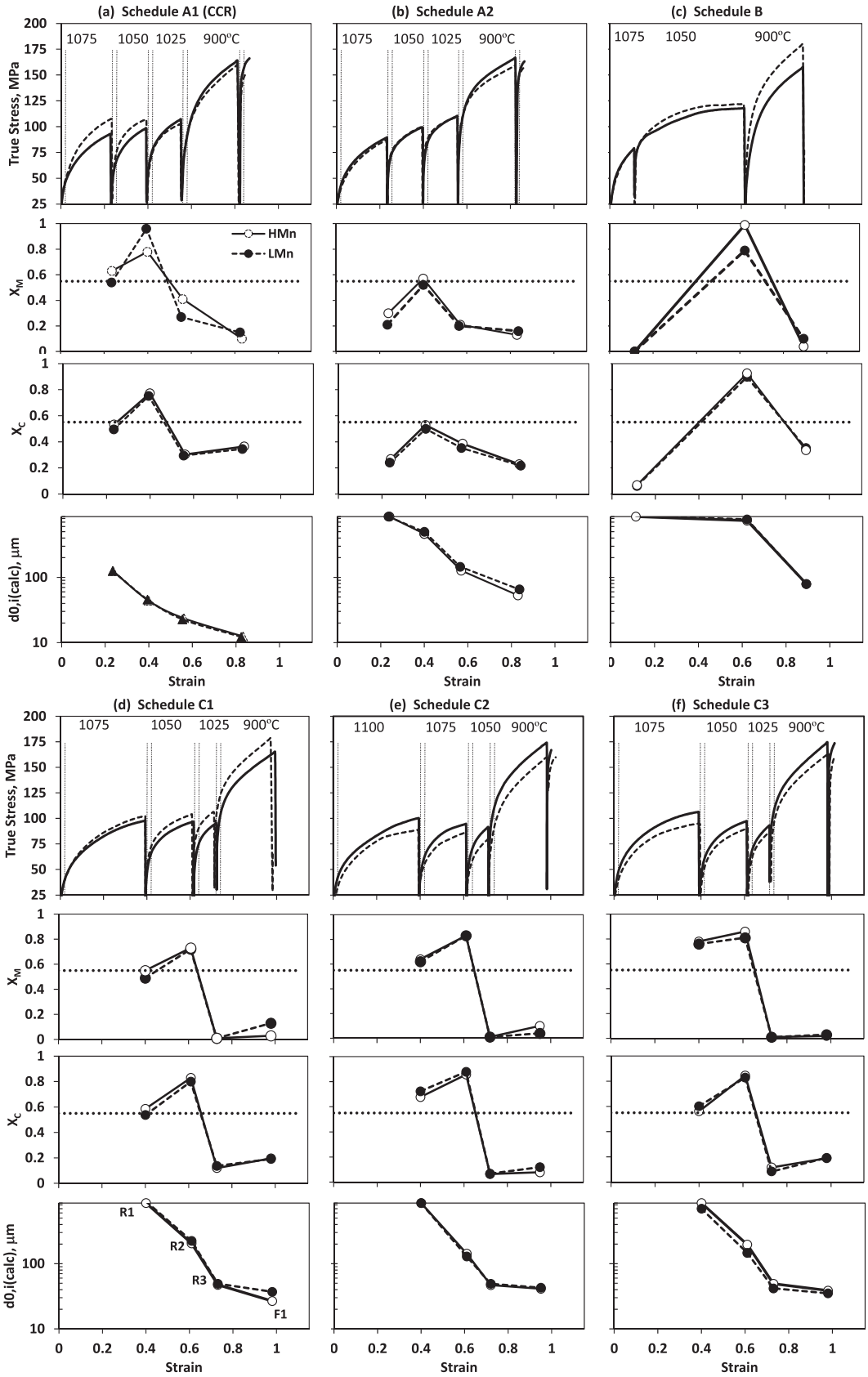

Fig. 3. Flow curves, X and $d_{0,i}$ in schedules A-C for F1 = 900°C. All schedules were subjected to a "chill" to T_{min} (950°C), except in C3 where specimens were cooled directly to the equalising temperature of 1 100°C.

to that found at the lower F1 temperature, Fig. 4(d), but the *HMn* grade was somewhat coarser at the higher F1 temperature. The $d_{0,2}$ was 204 μm.

3.2. Recrystallisation Model

The Nb and Ti solute contents in 0.09%Nb-0.01Ti steel, calculated from Thermocalc®, are shown in **Fig. 8** for Mn contents of 0.25% and 1.6%. The [Nb] for both chemistries

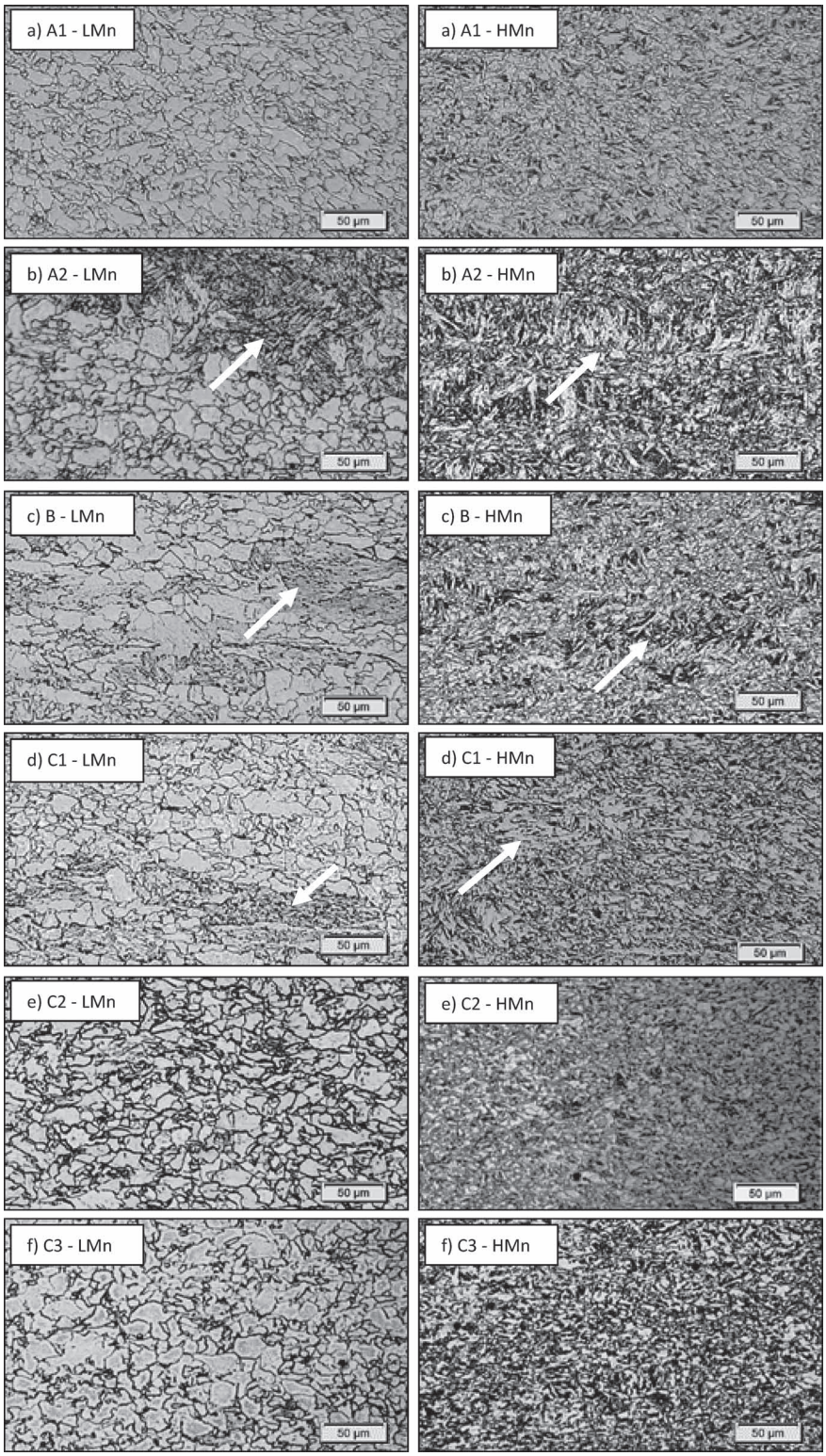

Fig. 4. "As-coiled" microstructures in *LMn* and *HMn* steels after schedules A–C (fig. 3). F1 = 900°C.

was calculated to be 0.047–0.06% at equalising temperatures between 1 100–1 125°C, *i.e.*, slightly less than half of the Nb has the potential to precipitate prior to rolling. The solute Ti content is close to zero in the roughing region. Coarse eutectic, plate-like Nb(C,N) precipitates, similar to those observed elsewhere[15] were present, **Fig. 9**, which reduce the solute content available for subsequent precipitation. Eutectic precipitates were assumed not to influence roughing behaviour as they are very coarse and occur at high temperatures. Thermocalc® predicted little influence of Mn on Nb solubility in austenite in these steels. In Fig. 3, the best-fit values between X_M and X_C for the constant C in Eq. (2) were 4.96×10^{-11} s and 4.51×10^{-11} s for *LMn* and *HMn* grades respectively, **Fig. 10**. The incorporation of retained strain into the effective strain after each pass was essential to obtain acceptable accuracy between X_M and X_C values.

3.3. Precipitation Studies

In schedule C, the earliest evidence of NbTi(C,N) pre-

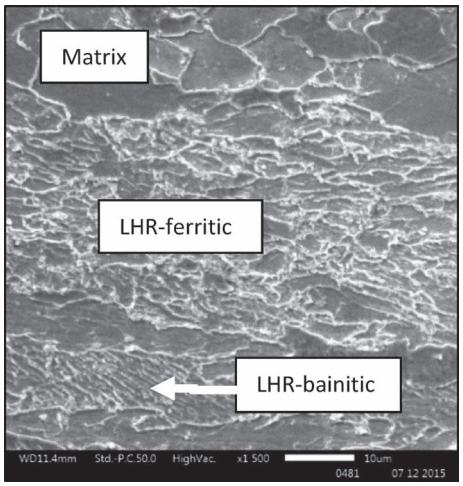

Fig. 5. SEM micrograph of LHR in "as-coiled "*LMn* steel. *cf.* Schedule C1.

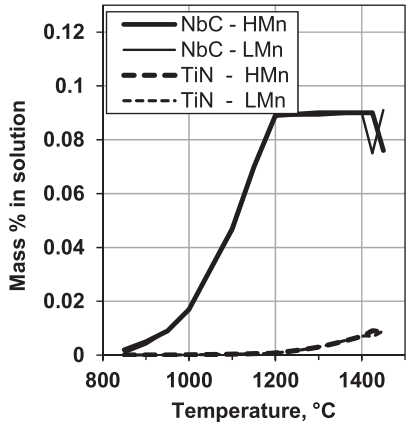

Fig. 8. Nb and Ti solute contents in 0.06%C-0.09%Nb-0.01%Ti-0.006%N steel as a function of temperature and Mn content as calculated using Thermocalc®.

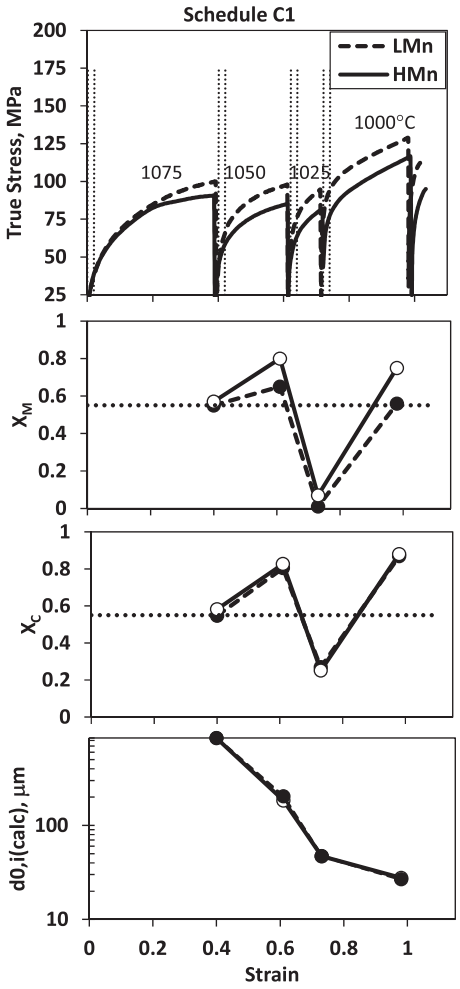

Fig. 6. Flow curves, X and $d_{0,i}$ in schedule C1 for F1 = 1 000°C.

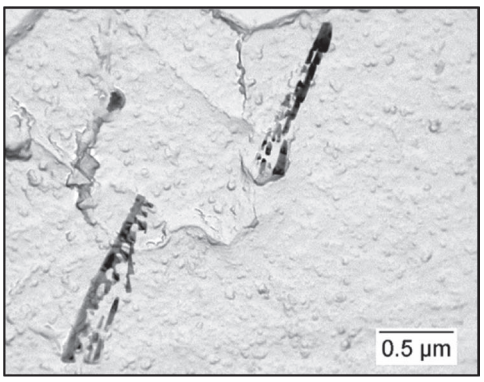

Fig. 9. TEM micrograph showing eutectic Nb precipitates in grade *HMn*, schedule C1, quenched from 1 100°C.

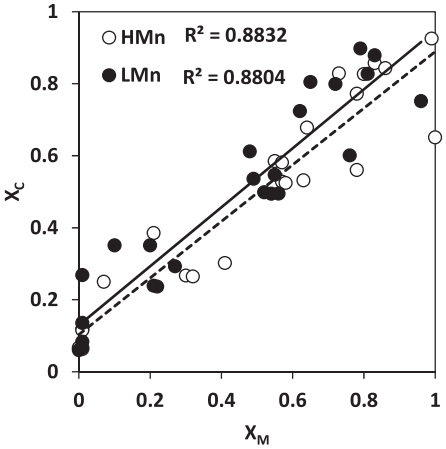

Fig. 10. Softened fraction X in passes R1 and R2 - all tests. Measured vs Calculated.

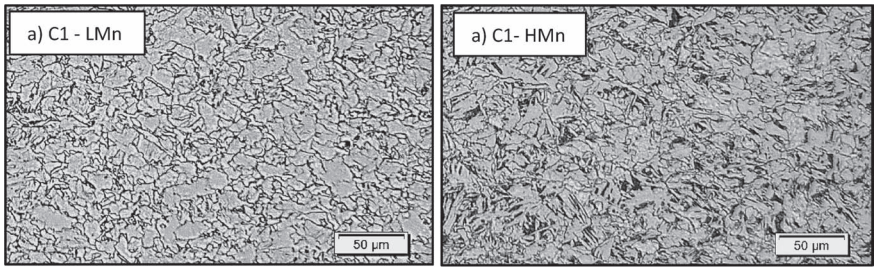

Fig. 7. "As-coiled" microstructures in *LMn* and *HMn* steels after schedule C1 (fig. 5). F1 = 1 000°C.

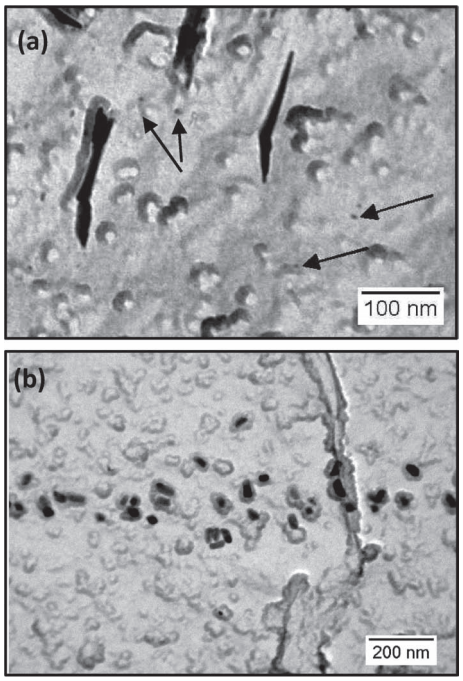

Fig. 11. TEM extraction replicas showing (a) fine (4–7 nm, arrows) matrix precipitation in *LMn* after cooling to T_{min} from 1 400°C and (b) Coarse, Nb,Ti(C,N) particles in *HMn* after R1, schedule C1.

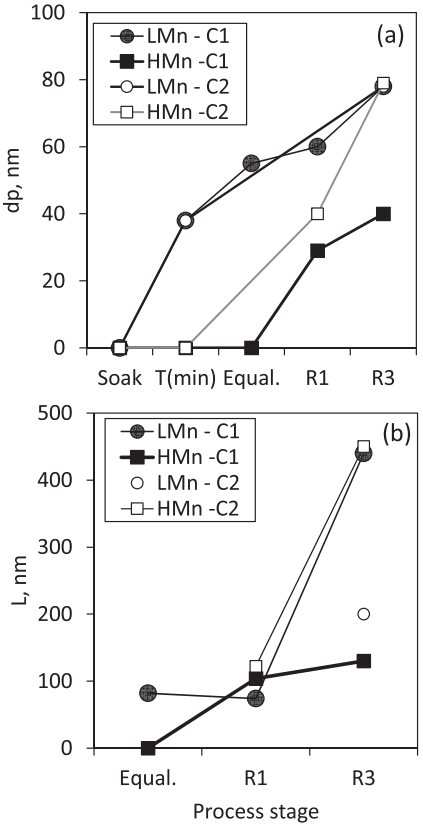

Fig. 12. Precipitate evolution in grades *LMn* and *HMn*. (a) d_p and (b) L measurements after schedules C1 and C2.

cipitation in low Mn grade *LMn* was found at T_{min}, Fig. 2, showing that fine (4–7 nm), undeformed precipitation preceded roughing, **Fig. 11**(a). Precipitation in the *HMn* steel was first detected after R1 in the case of schedule C1, Fig. 11(b). The d_p and L at various stages of schedules C1 and C2 are shown in **Fig. 12**. Figure 12(a) shows that in both *LMn* and *HMn*, d_p after R3 is above 30 nm. Occasionally, a high density of precipitation was observed on grain boundaries, as indicated by the small L values, Fig. 12(b). After R1, there is no evidence of d_p smaller than 5 nm, implying that nucleation is complete and only growth and coarsening occurred. Excluding the Nb eutectic phase, no precipitation was observed in either grade after direct cooling to 1 100°C.

4. Discussion

4.1. Particle Evolution and Pinning Force

Particles below 10 nm are generally coherent and effective for increasing flow stress,[16] retarding recovery, recrystallization and resisting dislocation motion. Fine precipitation in the 4–7 nm diameter range was detected prior to roughing only in *LMn*, Fig. 11(a), indicating that precipitation is more rapid compared to the *HMn* steel.

In the *HMn* steel the precipitates nucleate at the onset of deformation in R1 and coarsen to 30 nm in the 15 s inter-pass time - a growth rate similar to that predicted by Manohar.[17] However, the d_p after R1 is generally similar to the particle sizes present prior to equalization.[18] These particles are generally incoherent and do not affect recrystallization.

The lack of influence of precipitation was confirmed in **Fig. 13**(a), where no clear relationship between d_p and X_M was found. However, since large L appears to increase X, the combined effect of d_p and L were considered by evaluating particle pinning and recrystallisation forces. The driving force for grain boundary front migration during static recrystallization is $F_{REX} = \mu b^2 \Delta\varphi/2$ where μ is the shear modulus of austenite, b is the Burgers vector, and $\Delta\varphi$ is the change in dislocation density associated with the migration of the recrystallization front into the deformed region.[19] The formation of a high volume fraction, f, of fine precipitation of radius, r, resists this force on a flexible boundary[20] by exerting an opposing force, $F_{PIN} = 3\sigma f^{2/3}/\pi r$ where σ is the interfacial energy per unit area of boundary.[21] The driving force for recrystallisation increases when F_{REX} rises and when F_{PIN} decreases. Force – X plots in Fig. 13(b) for schedules C1 and C2 after pass R1 gave inverse relationships to those expected for both steels – *i.e.* higher F_{PIN} increases X and low F_{REX} increases X. Thus, Nb probably influences recrystallisation in solute form since no correlations between X and precipitate characteristics were found. This concurs with Kundu *et al.*[22] who found a stronger effect of solute drag than particle pinning in retarding recrystallisation in Nb steels at temperatures above 1 050°C, *i.e.*, during roughing.

4.2. Elimination of Local Heterogeneous Microstructure

As stated earlier, the overall, or bulk X should be above 0.55 in R1 and in at least one other pass, whether in roughing or early finishing. Theoretically however, X should approach unity to eliminate local heterogeneous regions. This disparity can, in part, be accounted for by considering the local strain distribution in both axisymmetric specimens and flat-rolled products for a given applied bulk strain. Szeliga[23] has shown that the local strain at the work piece centre is larger than the applied strain and the difference

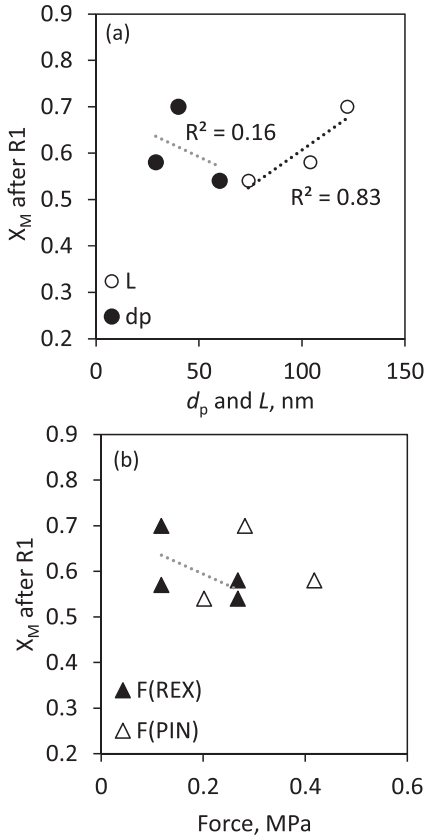

Fig. 13. (a) The influence of d_p and L on X after R1 showing no relationship between d_p and X but good correlation with L. (b) Weak relationships were found between F_{REX}, F_{PIN} and X after R1 for both steels in schedules C1 and C2.

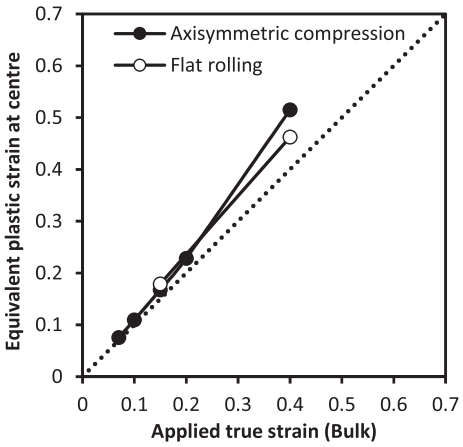

Fig. 14. FEM plot showing relationship between applied strain and centre strain (von Mises) in 5×10 mm^2 axisymmetric specimens and flat plate rolling.[23]

between the two strains increases with applied strain, but slightly less in flat rolling.[24] This was seen after ABAQUS ver. 6.11 FEM simulations in **Fig. 14**. Thus, it is expected that more recrystallization and a consequent decrease in local heterogenity occurs in the central regions. For *e.g.* applied strains of 0.2 and 0.4 produce localised strains of 0.25 and 0.52 respectively at the specimen centre. A local strain of 0.52 in schedule C2 is expected to result in an X_C of 0.89, compared to only 0.72 for a bulk strain of 0.4. Of course, subsequent passes with high X values provide additional energy to recrystallize the remaining local heterogeneous regions. Slow air cooling after roughing provides additional time at high temperatures for more extensive SRX and MDRX.

The extent of recrystallization in R1 is critical to eliminating local heterogeneous regions. This is clearly seen in schedule B, where even a very large applied strain (0.5) in R2, together with the retained strain from R1, provided a local central strain approaching 0.75 but does not eliminate local heterogeneous regions, despite the initiation of MDRX which is a more potent grain refining process than SRX. This is attributed to insufficient subsequent deformation for the so-called "necklacing" process to go to completion at coarse austenite grain boundaries inherited from R1.

It is not clear why the extent of softening in R1 is so high ($X_M > 0.75$) in both grades after direct cooling to the equalising temperature of 1 100°C in schedule C3, given the same d_0 as in schedules C1 and C2. A possible explanation is more homogeneous distribution of solute in the absence of grain boundary precipitation prior to R1 may facilitate easier recrystallisation.

Slow air cooling to a high F1 temperature of 1 000°C contributes to more extensive static recrystallisation which aids the elimination of local heterogenous regions. However, care must be taken if this route is adopted in the processing of thick HTP steels, since high temperature processing in the partial recrystallisation region may produce mixed final structures which compromises the final properties.

The cooling conditions after rolling may also be a determining factor regarding the presence of local heterogenous regions. In Fig. 5, ferritic and bainitic local heterogenous regions morphologies were identified. Whilst a fine local heterogenous region with ferrite microstructure may not affect, or indeed improve properties, a high hardenability (due to the large prior austenite grain size compared to the matrix), coupled with sufficiently fast cooling rates, can instead transform the local heterogenous regions to a low temperature transformation product, such as bainite, and impair toughness because the effective grain size of a local heterogenous region now becomes that of the coarse prior austenite grain.

4.3. Influence of Mn

The lower X_M values found in the *LMn* grade at roughing temperatures indicates slower recrystallization kinetics in low Mn steels. Akben *et al.*[7] found that when Mn is added to 0.035%Nb steel, the solubility of the carbonitride is increased, so that the rate and amount of precipitation at a given temperature and strain are decreased. Both higher Nb and increased Mn in solution contribute to the retardation of the softening processes. When Mn (or V, Mo) is added to a Nb steel, the activity coefficient of Nb increases but decreases those of C and N appreciably, producing a net retardation of precipitation and recovery.[7] Zurob *et al.*[8] found that low Mn is better at preventing static recrystallisation than high Mn steel, *i.e.*, strain accumulation is more pronounced in low Mn steels. Whilst these effects are desirable during finishing for austenite pancaking, it is harmful in roughing, where the prevention of recrystallization from going to completion promotes local heterogenous microstructure, particularly in coarse-grained as-cast austenite subjected to small/intermediate strains. The larger austenite

grain size in the low Mn steel during roughing, as suggested by the occasional bainitic morphology of "as-coiled" local heterogenous regions (the larger grain size providing greater hardenability), may also contribute to the slower recrystallisation kinetics in the *LMn* grade.

The *HMn* steel was expected to display higher flow stresses during roughing and early finishing. However, the stress magnitudes in the *LMn* grade were comparable to, and sometimes higher than, that observed in the *HMn* grade. An explanation for the relatively high deformation resistance in grade *LMn* is the potential formation of clusters, not precipitates, when solutes concentrations are low, *i.e.* low Mn, which will retard recovery in worked austenite and increase flow stress.[7)]

5. Conclusions

Roughing conditions necessary to avoid the formation of local heterogeneous regions have been established for HTP steels with an initial grain size of 850 μm. The following are concluded:

(1) Low Mn Nb–Ti steels experience more sluggish recrystallisation kinetics and are more vulnerable to forming local heterogeneous regions during roughing.

(2) To prevent local heterogenous microstructure if finishing commences at 900°C, sufficient effective strain is necessary to produce a bulk softened fraction of at least 0.55 in each of the first two roughing passes. If finishing commences at 1 000°C, slow air cooling from roughing provides additional time for recrystallisation to go to completion and so prevent the occurrence of local heterogenous regions.

(3) Maintaining the strand temperature as high as possible prior to the commencement of roughing encourages recrystallisation. A roughing start temperature of 1 100°C, as opposed to 1 075°C, significantly reduces the risk of forming local heterogenous regions.

(4) For the conditions tested, no correlation between softening fraction and carbonitride precipitate characteristics was found. Thus, the influence of Nb on austenite recrystallisation is expected to be due to either solute drag or solute clustering.

Acknowledgements

The authors are grateful to CBMM and Dr. Malcolm Gray of the Microalloyed Institute for financial support.

REFERENCES

1) K. M. Banks and R. Maubane: Proc. Advanced Steel Metallurgy: Products and Processing, MS&T14, TMS, Warrendale, PA, (2014), 453.
2) M. Imagumbai and H. Takechi: Proc. Int. Conf. on Processing and Manufacturing of Advanced Materials (Thermec 2003), eds. by T. Chandra *et al.*, Trans Tech Publications, Zurich, (2003), 426.
3) K. M. Banks and R. Maubane: Conf. Proc. HSLA Steel 2015, Microalloying 2015 and Offshore Engineering, Steels 2015, Chinese Society for Metals and Chinese Academy of Engineering, Beijing, (2015), 783.
4) P. Uranga, A. I. Fernández, B. López and J. M. Rodriguez-Ibabe: *ISIJ Int.*, **44** (2004), 1416.
5) Y. Sha, Z. Q. Sun and L. F. Li: *Ironmaking Steelmaking*, **42** (2015), No. 1, 74.
6) J. M. Gray and F. Barbarro: Conf. Proc. HSLA Steel 2015, Microalloying 2015 and Offshore Engineering Steels 2015, Chinese Society for Metals and Chinese Academy of Engineering, Beijing, (2015), 53.
7) M. G. Akben, B. Bacroix and J. J. Jonas: *Acta Metall.*, **31** (1983), 161.
8) H. S. Zurob, G. Zhu, S. V. Subramanian, G. R. Purdy, C. R. Hutchinson and Y. Brechet: *ISIJ Int.*, **45** (2005), 713.
9) A. I. Fernández, P. Uranga, B. López and J. M. Rodriguez-Ibabe: *ISIJ Int.*, **40** (2000), 893.
10) P. Uranga, A. I. Fernández, B. López and J. M. Rodriguez-Ibabe: *Mater. Sci. Eng. A*, **345A** (2003), 319.
11) R. Abad, A. I. Fernández, B. López and J. M. Rodriguez-Ibabe: *ISIJ Int.*, **41** (2001), 1375.
12) C. Roucoules, S. Yue and J. J. Jonas: *Metall. Mater. Trans. A*, **26A** (1995), 181.
13) P. Uranga, A. I. Fernández, B. López and J. M. Rodriguez-Ibabe: Proc. 44th MWSP Conf., Vol. 40, ISS, Warrendale, PA, (2002), 945.
14) F. Siciliano and J. J. Jonas: *Metall. Mater. Trans. A*, **31A** (2000), 511.
15) O. Hunderi and N. Ryum: *Acta Metall. Mater.*, **40** (1992), 543.
16) T. Greday and M. Lamberigts: Proc. Conf. Microalloying '75, Union Carbide Corporation, New York, (1977), 172.
17) P. A. Manohar, D. P. Dunne, T. Chandra and C. R. Killmore: *ISIJ Int.*, **36** (1996), 194.
18) A. Ruiz-Aparicio: MSc Dissertation, University of Pittsburgh, (2004), http://d-scholarship.pitt.edu/7913/1/ARTURORUIZAPARICIO.pdf, (accessed 2015-09-02).
19) U. F. Kocks, A. S. Argon and M. F. Ashby: Progress in Materials Science, Vol. 19, ed. by B. Chalmers, Pergamon Press, Oxford, (1975), 1.
20) E. J. Palmiere, C. I. Garcia and A. J. DeArdo: *Metall. Mater. Trans. A*, **27A** (1996), 951.
21) L. Cuddy: Thermomechanical Proc. Microalloyed Austenite, eds. by A. J. DeArdo, *et al.*, TMS-AIME, Warrendale, PA, (1982), 129.
22) A. Kundu: Ph.D. thesis, The University of Birmingham, (UK), (2011), https://core.ac.uk/download/files/121/1631723.pdf, (accessed 2015-11-03).
23) D. Szeliga, R. Kuziak, R. Kopp, G. Smyk and M. Pietrzyk: *Arch. Metall. Mater.*, **60** (2015), No. 4, 3087.
24) M. Pietryzyk and J. G. Lenard: Thermal-Mechanical Modelling of the Flat Rolling Process, MRE, eds. by B. Ilschner and N. J. Grant, Springer-Verlag, Berlin, Heidelberg, (1991), 161.